The Astronomical Journal, 139:1190–1198, 2010 March doi:10.1088/0004-6256/139/3/1190

AN INVESTIGATION OF THE DUST CONTENT IN THE GALAXY PAIR NGC 1512/1510 FROM NEAR-INFRARED TO MILLIMETER WAVELENGTHS

Guilin Liu[1], Daniela Calzetti[1], Min S. Yun[1], Grant W. Wilson[1], Bruce T. Draine[2], Kimberly Scott[1], Jason Austermann[1,3], Thushara Perera[1], David Hughes[4], Itziar Aretxaga[4], Kotaro Kohno[5,6], Ryohei Kawabe[7], and Hajime Ezawa[7]

[1] Astronomy Department, University of Massachusetts, Amherst, MA 01003, USA; gliu@astro.umass.edu, calzetti@astro.umass.edu, myun@astro.umass.edu, wilson@astro.umass.edu, kscott@astro.umass.edu, jaustermann@gmail.com, thusharaprr@gmail.com

[2] Department of Astrophysical Sciences, Princeton University, Princeton, NJ 08544, USA; draine@astro.princeton.edu

[3] Center for Astrophysics and Space Astronomy, University of Colorado, Boulder, CO 80309, USA

[4] Instituto Nacional de Astrofísica, Óptica y Electrónica (INAOE), Aptdo. Postal 51 y 216, 72000 Puebla, Mexico; dhughes@inaoep.mx, itziar@inaoep.mx

[5] Institute of Astronomy, University of Tokyo, 2-21-1 Osawa, Mitaka, Tokyo 181-0015, Japan; kkohno@ioa.s.u-tokyo.ac.jp

[6] Research Center for the Early Universe, University of Tokyo, 7-3-1 Hongo, Bunkyo, Tokyo 113-0033, Japan

[7] Nobeyama Radio Observatory, National Astronomical Observatory of Japan, Minamimaki, Minamisaku, Nagano 384-1305, Japan; ryo.kawabe@nao.ac.jp, h.ezawa@nao.ac.jp

Received 2009 July 28; accepted 2009 December 23; published 2010 February 11

ABSTRACT

We combine new ASTE/AzTEC 1.1 mm maps of the galaxy pair NGC 1512/1510 with archival *Spitzer* IRAC and MIPS images covering the wavelength range 3.6–160 μm from the SINGS project. The availability of the 1.1 mm map enables us to measure the long-wavelength tail of the dust emission in each galaxy, and in sub-galactic regions in NGC 1512, and to derive accurate dust masses. The two galaxies form a pair consisting of a large, high-metallicity spiral (NGC 1512) and a low-metallicity, blue compact dwarf (NGC 1510), which we use to compare similarities and contrast differences. Using the models of Draine and Li, the derived total dust masses are $(2.4 \pm 0.6) \times 10^7\ M_\odot$ and $(1.7 \pm 3.6) \times 10^5\ M_\odot$ for NGC 1512 and NGC 1510, respectively. The derived ratio of dust mass to H I gas mass for the galaxy pair, $M_d/M_{\rm H\,I} \sim 0.0034$, is much lower (by at least a factor of 3) than expected, as previously found by Draine et al. In contrast, regions within NGC 1512, specifically the central region and the arms, do not show such unusually low $M_d/M_{\rm H\,I}$ ratios; furthermore, the dust-to-gas ratio is within expectations for NGC 1510. These results suggest that a fraction of the H I included in the determination of the $M_d/M_{\rm H\,I}$ ratio of the NGC 1512/NGC 1510 pair is not associated with the star-forming disks/regions of either galaxy. Using the dust masses derived from the models of Draine & Li as references, we perform simple two-temperature modified blackbody fits to the far-infrared/millimeter data of the two galaxies and the sub-regions of NGC 1512, in order to derive and compare the dust masses associated with warm and cool dust temperature components. As generally expected, the warm dust temperature of the low-metallicity, low-mass NGC 1510 ($T_w \sim 36$ K) is substantially higher than the corresponding warm temperature of the high-metallicity spiral NGC 1512 ($T_w \sim 24$ K). In both galaxies (albeit with a large uncertainty for NGC 1510), our fits indicate that a substantial fraction (>93%) of the total dust mass is in a cool dust component, with temperatures ∼14–16 K for NGC 1512 and ∼15–24 K for NGC 1510. This result is similar to what is determined for a few other nearby galaxies. In contrast, the warm dust component in the sub-galactic regions of NGC 1512 represents a much larger fraction of the total dust content, in agreement with the fact that all three regions have higher specific star formation rates than the average in the galaxy; in the center, the warm dust represents about 40% of the total, while in the arms the fractions are close to ∼20%.

Key words: dust, extinction – galaxies: individual (NGC1510, NGC1512) – galaxies: ISM – galaxies: starburst

1. INTRODUCTION

Interstellar dust provides a source of attenuation of the light from galaxies, but also a source of information on their metal content, and, possibly, a tracer for the molecular gas content (Draine et al. 2007). On average, about 50% of the UV–optical light from galaxies is reprocessed by their own dust into the mid/far-infrared and millimeter wavelength range (Dole et al. 2006).

Determining accurate dust masses for galaxies has been, traditionally, a difficult step since measurements at infrared wavelengths shorter than ∼100–200 μm (as accomplished by *IRAS*, the *Infrared Space Observatory*, and the *Spitzer Space Telescope*) are sensitive to the inferred dust mean temperature(s) and the adopted dust emissivity. Wavelengths longer than a few hundred μm probe the long-wavelength tail of the modified Planck function for typical galaxy dust emission, and the inferred dust masses are, therefore, less sensitive to the dust temperature. Long-wavelength measurements also offer additional leverage for constraining, when used together with shorter wavelength infrared data, the dust temperature itself.

Recent applications of submillimeter data used to constrain the properties of the dust emission from galaxies include a nearby sample of about 100 galaxies observed at 450 μm and 850 μm with SCUBA (SLUGS, Dunne et al. 2000; Dunne & Eales 2001; Seaquist et al. 2004; Vlahakis et al. 2005), and an additional ∼20 galaxies from the SINGS sample (Kennicutt et al. 2003), where *Spitzer* data in the range 3–160 μm have been combined with SCUBA 850 μm detections (Draine et al. 2007). More recently, submillimeter data have been combined with *Spitzer* data for 11 nearby galaxies from the SLUGS sample (Willmer et al. 2009), thus increasing the total number of galaxies for which the dust masses are measured accurately from multi-wavelength spectral energy distributions (SEDs), spanning from the mid-IR to the submillimeter. The SLUGS galaxies tend to have, on average, colder dust temperatures than

Table 1
Characteristics of the Galaxies

Characteristic	NGC 1512	NGC 1510
Morphology[a]	SB(r)ab	$SA0^0$ pec?; H II BCDG
v_H (km s^{-1})	898 ± 3	913 ± 10
D (Mpc)[b]	10.8 ± 0.8	11.0 ± 0.8
12+log(O/H)[c]	8.71	8.31
Σ_{SFR}[d]	0.001	0.06

Notes.
[a] Galaxy morphology and heliocentric velocity are from the NASA/IPAC Extragalactic Database (NED).
[b] Adopted distances.
[c] Oxygen abundances, from Moustakas et al. (2009) for NGC 1512 and from Storchi-Bergmann et al. (1994) for NGC 1510.
[d] The star formation rate density, in units of $M_\odot$ yr^{-1} kpc^{-2}, from a combination of Hα and 24 μm measurements for NGC 1512, to account for both the dust obscured and unobscured star formation (Kennicutt et al. 2009), and from Hα measurements for NGC 1510 (Calzetti et al. 2009).

the galaxies in the SINGS sample (of which NGC 1512/1510 is part), as estimated by Willmer et al. (2009) on the basis of the far-infrared/submillimeter colors.

The *Spitzer* data on nearby galaxies offer the unique opportunity to analyze the dust emission characteristics not only of whole galaxies, but also within sub-galactic regions, thanks to its angular resolution in the range 2″–38″ for the 3–160 μm range. We combine the SINGS data on the interacting galaxy pair NGC 1512/1510 with data at 1.1 mm wavelength from ASTE/AzTEC, which has 28″ resolution, to investigate the infrared/millimeter SED of dust for those two galaxies, and for regions within the larger NGC 1512. Our goal is to derive accurate dust masses for the two galaxies, and to compare the SEDs between sub-regions.

The interacting pair NGC 1512/1510 is of particular interest because its two member galaxies are remarkably distinct in nature: the primary galaxy, NGC 1512, is a large, metal-rich barred spiral, while its companion, NGC 1510, is a low-metallicity blue compact dwarf (BCD) galaxy (Table 1) which is expected to have less ability of self-shielding for the dust. Both galaxies are characterized by intense starburst activity in their central regions, and do not show evidence for presence of active galactic nuclei. This pair is thus ideal for investigations of dust SEDs, and their dependence on each galaxy's properties.

The paper is organized as follows: Section 2 describes the data and, for the ASTE/AzTEC data, provides some detail on the observations and data reduction; Section 3 is devoted to the data analysis, including the photometry, and photometric corrections and uncertainties; Section 4 presents the dust model fitting and results; and the discussion and conclusions are in Section 5.

2. DATA

2.1. IRAC and MIPS Data

Spitzer maps with both the IRAC (3.6, 4.5, 5.8, and 8.0 μm) and MIPS (24, 70, and 160 μm) are available for both galaxies, through the high level data products of the SINGS Legacy project (Kennicutt et al. 2003). Although the SINGS observations targeted NGC 1512 only, its companion galaxy is serendipitously present and detected in the same maps. The SINGS observation strategy, data reduction procedures, and map sensitivity limits are described in Kennicutt et al. (2003) and Dale et al. (2005). The angular resolution is ∼2″ for the four IRAC bands and 6″, 17″, and 38″ for the MIPS 24, 70, and 160 μm bands, respectively (Figure 1).

2.2. AzTEC/ASTE Data

AzTEC is a 144 element bolometer array currently configured to observe in the 1.1 mm atmospheric window (Wilson et al. 2008a). Observations of NGC 1512 were made with AzTEC on the Atacama Submillimeter Telescope Experiment (ASTE;

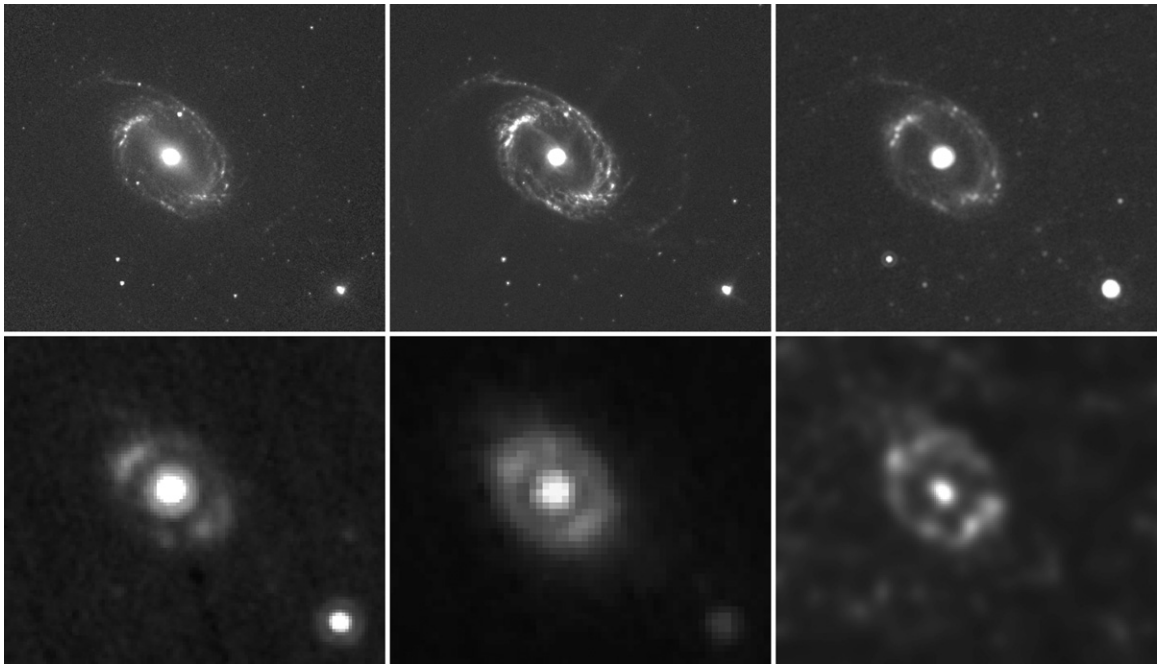

Figure 1. Mosaic of the images of the galaxy pair NGC 1512/NGC 1510 at 5.8, 8.0, 24, 70, 160 μm and 1.1 mm. North is up; east is left. The field of view of each panel is 8′.7 × 7′.4.

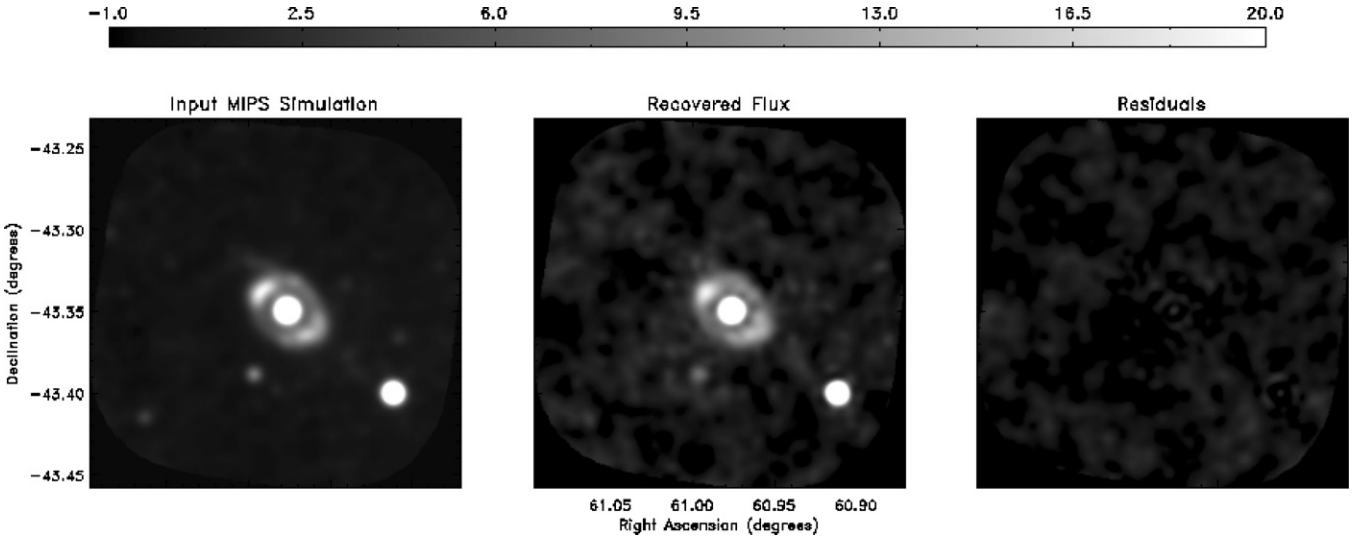

Figure 2. Left panel: input MIPS 24 μm image scaled such that the extended flux matches that measured in the AzTEC map. This results in a peak flux at the galaxy center of 133 mJy. This image is injected into the residual AzTEC timestreams as described in the text. Middle panel: recovered image using the same FRUITLOOPS algorithm as used to produce the AzTEC image of NGC 1512/1510. Right panel: residual image (left image minus middle image). Negligible artifacts of 1–2 mJy from the AzTEC analysis filters remain in the cores of the two galaxies due to the bright initial image flux. The faint extended flux is recovered to well within the pixel noise of the map.

Ezawa et al. 2004, 2008) using a network observation system N-COSMOS3 (Kamazaki et al. 2005), which provided a 28″ circular main beam. During the period 2007 October 7–11, we performed 25 Lissajous observations identical to those described in Wilson et al. (2008b) centered on ($04^{h}03^{m}54\overset{s}{.}28$, $-43^{\circ}20'55\overset{''}{.}9$). The co-addition of the 25 observations results in a roughly circular map with uniform coverage over the central 18′ diameter with a depth of ≈1.5 mJy. The structure of NGC 1512 is well resolved, with a maximum signal-to-noise ratio (S/N) ∼10 in the core, and ∼8 on the arms; its companion, NGC 1510, is detected with only marginal significance with a peak S/N of ∼3.5 (Figure 1).

Atmospheric emission at 1.1 mm is the dominant noise source in our AzTEC maps. Previous images made with the standard AzTEC pipeline (Scott et al. 2008; Perera et al. 2008) are optimized for point source recovery and consequently do not preserve extended flux in the image. We have developed our own iterative flux recovery technique that takes advantage of the fact that the atmospheric noise is not correlated between the 25 observations and that the atmosphere is transient in time while the astronomical signal is stationary. We begin by using a variant of the principal component analysis (PCA) technique described in Scott et al. (2008) to remove atmosphere from the detector timestreams. Rather than the aggressive form of filtering described there—which would result in a sharp spatial filter applied to this map—we project just two eigenmodes from the detector–detector correlation matrix out of each 15 s span of time-ordered data. This relatively weak filter is comparable in strength to a subtraction of the array average and gradient from each detector timestream sample. Once these initial "cleaned" data streams are produced, we implement the following algorithm.

1. A co-added image of the field is made from the cleaned data streams.
2. The fluxes from pixels within 24″ of pixels with S/N > 2.5 are preserved in the cleaned image while all other pixels are set to zero. We call this the "current best sky" image since it is the best estimate we have of a (noiseless) sky.
3. The "current best sky" image is recast into the timestreams of the detectors and subtracted from the original detector timestreams, creating a set of residual timestreams that, in principle, have the same contamination from the atmosphere but less true astronomical signal. We call these the "residual observations."
4. The "residual observations" are cleaned and mapped. The resulting image is added to the "current best sky" image and a new "current best sky" realization is produced using the same pixel flux criteria as before.
5. This iterative process continues until no new pixels in the realization pass the pixel flux criteria.
6. At this point, the severity of atmospheric filtering is increased. That is, another detector–detector covariance matrix eigenvector is projected out of the PCA basis for the atmospheric cleaning and the iterations continue.
7. Iterations are complete when the full PCA technique for optimal point source detection is realized (in this case, cutting seven eigenmodes in the atmosphere cleaning step) and no new pixels pass the pixel flux criteria (Scott et al. 2008).

One benefit of this technique is that it results in a set of 25 residual timestreams that have been effectively "cleared" of astronomical signal while leaving a good approximation of the true atmospheric contamination behind. We take advantage of this by injecting various forms of simulated signals into these residual timestreams in order to perform tests on the effectiveness of the iterative flux recovery technique. Figure 2 shows the results of injecting a flux-scaled version[8] of the MIPS 24 μm map of NGC 1512, smoothed with a 28″ Gaussian, into our residual timestreams and then repeating the identical analysis that was done for the AzTEC NGC 1512 observations. The residual map is consistent with the noise level in the AzTEC

[8] The flux of the MIPS map has been scaled such that the extended features of the galaxy have a flux that matches that of the AzTEC NGC 1512 map. This results in a peak flux in the core of the galaxy which is significantly larger than what we actually see at 1.1 mm, so this is a robust test of the iterative flux recovery technique.

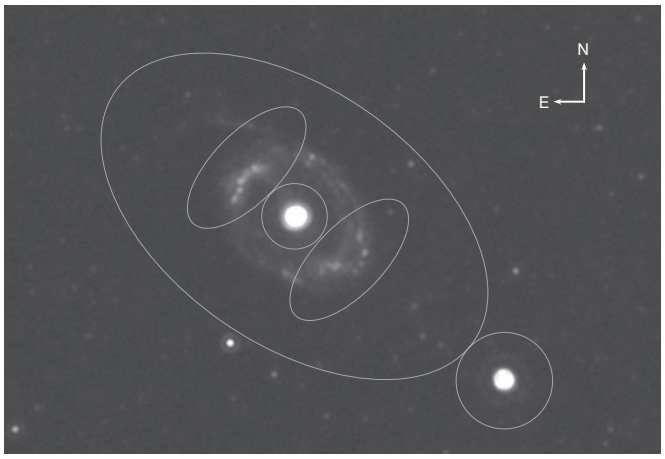

Figure 3. Five photometric apertures used in this paper are shown as ellipses/circles, superimposed on the 24 μm map of the galaxy pair. The field of view is $11.'4 \times 8.'5$.

NGC 1512 image and shows only minor residual systematics of order 1–2 mJy at the locations of the cores of NGC 1510 and NGC 1512. We perform the same aperture photometry analysis on the residual map shown in Figure 2 as is done for the actual map (see Section 3.3) and find that our iterative flux recovery technique misses between 0.2% and 12% of the integrated flux depending on the scale-size of the aperture. These values are small compared to the total integrated flux and calibration uncertainty (17.1%–128%, see the next section).

3. DATA ANALYSIS

3.1. Photometric Apertures

In addition to measuring the fluxes from the whole galaxies, the infrared and millimeter maps have sufficient angular resolution to allow us to isolate substructures within the larger of the two galaxies, NGC 1512. We thus identify three separate sub-regions in this galaxy: the center, and two areas in the spiral arms (Figure 3). For each of these regions, we define circular or ellipsoidal apertures, depending on the structure we are measuring.

For NGC 1512 as a whole, we define an elliptical aperture (Figure 3), with major/minor axes $491''/287''$ and centered on the galaxy position defined in NASA/IPAC Extragalactic Database (NED)[9]; the aperture's major and minor axes are matched to the optical major and minor axes and the position angle extracted from the KPNO/Cerro Tololo Inter-American Observatory (CTIO) *BVRI* imaging campaign for the SINGS project (Table 1 of Dale et al. 2007). For NGC 1510, which is unresolved in the MIPS and millimeter images, and only marginally resolved in the IRAC bands, we define a single, circular aperture, with diameter $108.''4$, centered again on the NED position of the galaxy.

The size and location of the photometric apertures for the substructures in NGC 1512 are more arbitrary in nature, and we define them based on the 1.1 mm map, taking also into account the lower resolution of the 160 μm image. The central region is defined by a circular aperture centered on the NED galaxy center, and with diameter $73.''6$, delimited by the size of the central emission region which is similar in the maps of the two longest wavelengths. The location and size of the two apertures along the spiral arms (Figure 3) are chosen to encompass as much as possible of the northeastern and southwestern arm regions, while minimizing overlap with the central region. The arm apertures are thus elliptical in shape with major/minor axes $174''/78''$.

A constant background is determined and subtracted from each *Spitzer* image, using the peak value of the background pixels distribution (see description in Calzetti et al. 2005). The 1σ uncertainty of the background band is, in units of MJy sr^{-1}, [0.008, 0.012, 0.052, 0.053] for IRAC [3.6, 4.5, 5.8, 8.0] μm, and [0.039, 0.36, 0.48] for MIPS [24, 70, 160] μm, respectively. After background subtraction, photometric values are determined for each of the five regions in each band.

3.2. Photometric Corrections

Our photometric measurements require a few corrections, due to the presence of MIPS flux non-linearities, point-spread function (PSF) wings outside the apertures, and, for IRAC, scattered light for extended sources.[10] 1.1 mm ASTE/AzTEC data require no aperture corrections.

MIPS 70 μm pixels with surface brightness above $\sim$66 MJy sr^{-1} are subject to non-linearities that need to be corrected. The central pixel of NGC 1512 is above this threshold, and we adopt the non-linearity correction formula published in Dale et al. (2007; Equation (3)), which is deduced from data given in Gordon et al. (2007). A correction factor of 1.011 is derived for the photometry of the whole galaxy, and 1.023 for its central region.

The extended source aperture corrections provided by the Spitzer Science Center for IRAC gives [0.911, 0.941, 0.798, 0.745] for NGC 1512, [0.928, 0.960, 0.901, 0.791] for its central region, [0.919,0.949, 0.866, 0.770] for the north arm, [0.919, 0.949, 0.866, 0.770] for the south arm, and [0.920, 0.950, 0.869, 0.771] for NGC 1510 at [3.6, 4.5, 5.8, 8.0] μm, respectively, with an average uncertainty $\sim$10%.

We adopt the MIPS aperture corrections ([1.04, 1.05, 1.06] at [24, 70, 160] μm for NGC 1512 given in Dale et al. (2007). For the other apertures, we evaluate the corrections by measuring the wings of MIPS PSFs for the relevant aperture sizes. The aperture correction for the central region of NGC 1512 and for NGC 1510 are [1.06, 1.13, 1.53] and [1.04, 1.08, 1.34] at [24, 70, 160] μm, respectively. We derive aperture corrections of [1.04, 1.08, 1.28] for the arm regions, which are roughly extrapolated from circular apertures inscribed and circumscribed to the minor and major axes, respectively, of the aperture ellipses.

3.3. Uncertainties

IRAC Calibration uncertainties are 5%–10% for 3.6 and 4.5 μm bands and 10%–15% for 5.8 and 8.0 μm bands (Dale et al. 2007). To be conservative, in this analysis we employ the upper limits of those ranges. For MIPS data, 4%, 7%, and 12% are adopted at 24, 70, and 160 μm, respectively (Engelbracht et al. 2007; Gordon et al. 2007; Stansberry et al. 2007). The AzTEC/ASTE 1.1 mm image calibration has an uncertainty of $\sim$8%.

Aperture corrections are $\sim$10% uncertain for IRAC channels. For the MIPS bands, the aperture correction uncertainties are as small as a few percent, and our estimates of [5%, 5%, 8%] at [24, 70, 160] μm are close to previous estimates (Dale et al. 2007).

[9] The NED is operated by the Jet Propulsion Laboratory, California Institute of Technology, under contract with the National Aeronautics and Space Administration.

[10] http://spider.ipac.caltech.edu/staff/jarrett/irac/

Table 2
Photometric Measurements of the Galaxy Pair NGC 1512/1510

λ (μm)	NGC 1512	NGC 1512$_{C}$[a]	NGC 1512$_{NE}$[a]	NGC 1512$_{SW}$[a]	NGC 1510
3.6 (mJy)	349 ± 49	147 ± 21	54 ± 8	52 ± 7	17 ± 2
4.5 (mJy)	220 ± 31	93 ± 13	34 ± 5	33 ± 5	11 ± 2
5.7 (mJy)	244 ± 44	107 ± 19	49 ± 9	45 ± 8	10 ± 2
7.9 (mJy)	394 ± 71	153 ± 28	82 ± 15	79 ± 14	19 ± 3
23.7 (mJy)	447 ± 29	202 ± 13	78 ± 5	73 ± 5	136 ± 9
71.4 (Jy)	6.24 ± 0.54	3.24 ± 0.28	1.03 ± 0.09	0.81 ± 0.07	1.04 ± 0.09
156 (Jy)	21.3 ± 3.1	6.65 ± 0.96	4.99 ± 0.72	4.68 ± 0.68	0.98 ± 0.14
1100 (mJy)	322 ± 55	34 ± 7	62 ± 15	56 ± 15	10 ± 12

Note. [a] NGC 1512$_{C}$ represents the central region of NGC 1512, while the northeastern/southwestern arms are denoted by NGC 1512$_{NE}$/NGC 1512$_{SW}$.

The background noise levels in the *Spitzer* images are found by performing a Gaussian fit of the pixel-value distributions. For the millimetric image, we test for false detections and fluctuations by performing photometry of the background in the map using ∼8000 slightly displaced consecutive apertures (with the same area as each of the apertures used for source photometry) to cover the whole image, but excluding sources and the map edges. A Gaussian fit is then applied on the resultant histogram of "background" photometry and the dispersion of the background fluctuation is obtained accordingly. This strategy results in relative 1σ total uncertainties at 1 mm (errors in absolute flux calibration and background estimation added in quadrature) of 17.1% (whole), 20.9% (core), 24.8% (northeast arm), and 26.7% (southwest arm) for NGC 1512, and 128% for the entire NGC 1510. Total uncertainties computed in this fashion are listed in Table 2 for all the IRAC, MIPS, and AzTEC bands.

4. MODEL FITTINGS AND RESULTS

The silicate–graphite–PAH dust model of Draine & Li (2007) is used to fit, via χ^2 minimization, the flux densities of the two galaxies and of three sub-galactic regions in all eight bands. Parameters in the models are the PAH mass fraction $q_{\rm PAH}$, the lower cutoff of the starlight intensity distribution, and the fraction of the dust heated by starlight. The dust composition is assumed to be a mixture of carbonaceous grains and amorphous silicate grains, with size distributions consistent with the observed extinction curve in the local Milky Way (Weingartner & Draine 2001), along with varying amounts of PAH molecules. All charged PAHs (singly or multiply, positively or negatively) of a given size are assumed to have the same cross sections, but those of neutral and ionized PAHs are assumed to be different. This model employs a fixed shape for the PAH size distribution, a fixed PAH ionized fraction, and a fixed spectral shape of the illuminating starlight, which result in fixed ratios of PAH emission band strength. The stellar continuum contributing to the mid-infrared emission is approximated by a 5000 K blackbody (Draine & Li 2007).

The comparison between data and best-fit models are shown in Figure 4, together with the resulting model parameters. The SEDs of NGC 1512 and its regions are well represented by the models, yielding dust masses $M_d \sim 2.4 \times 10^7\ M_\odot$ for the whole galaxy, and in the range ∼2–6 $\times 10^6\ M_\odot$ for the regions within the galaxy (see Table 3), using the distance listed in Table 1. NGC 1510 is less well fit by the model, mainly owing to the combination of a high 70/160 μm ratio (which implies a high effective dust temperature) together with a highly uncertain 1.1 mm flux (whose value would imply presence of large amounts of cooler dust, see below). Despite the uncertainties, the models still provide a reasonable fit to the NGC 1510 SED, with a resulting dust mass $M_d \sim 1.7 \times 10^5\ M_\odot$, or about 150 times less dust mass than its companion galaxy. This difference is reduced to a factor of 45, if we use the upper bound of the large uncertainty in NGC 1510's dust mass determination.

As a test, we have also fit the far-infrared (70 and 160 μm) and millimeter data to a very simple prescription of two modified blackbodies, with temperatures and relative intensities derived through χ^2 minimization (Table 4). The power-law index of the dust emissivity is fixed to the value $\epsilon = 2$, following the conclusions of both Dunne & Eales (2001) and Willmer et al. (2009) who determine that this value produces better fits to the SEDs of the galaxies they consider lower than power-law index values. Overall, this is a very crude prescription, with four free parameters (warm dust temperature, T_w, cool dust temperature, T_c, the relative contribution of the two dust components to the observed infrared–millimeter SED, and the total luminosity), thus the fit is not constrained by our three data points (70 μm, 160 μm, and 1.1 mm). Indeed, we only derive these quantities for comparison purposes. However, in order to guide our physical intuition, we use the masses derived through the physical models of Draine & Li (2007) as our "target values" for the simple two-temperature prescription. For both galaxies and all regions, we find that the colder of the two temperatures is in the range $T_c \sim$ 14–16 K (Table 4). As a comparison, within the context of Draine & Li (2007) model, seeing that stronger radiation fields result in hotter dust grains, the lowest dust temperature can be inferred from the lower cutoff of the starlight intensity distribution $U_{\rm min}$. The best-fit model of the whole NGC 1512 is parameterized by $U_{\rm min} = 0.7$, corresponding to a lowest dust temperature ∼16 K, which is consistent with our result of two-temperature fittings as mentioned above. While for NGC 1510, $U_{\rm min} = 8.0$ and therefore a lower temperature limit is found to be 24 K, which is somewhat higher than that of the cooler dust component (∼15 K) obtained with the two-temperature fitting strategy. However, we do not regard this as a discrepancy, given that the 1.1 mm data point of NGC 1510 is highly uncertain and that both temperature values are still consistent with the fact that active star-forming galaxies appear to have cool dust components with temperatures of order 20 K (see the Discussion section). For the warmer dust component, we have a markedly different behavior for the two galaxies: NGC 1512 and its regions are described by "warm" dust temperatures in the range $T_w \sim$ 20–25 K, with the higher value being associated with the central region of the galaxy; NGC 1510 requires a warmer temperature than NGC 1512, $T_w \sim 36$ K, to

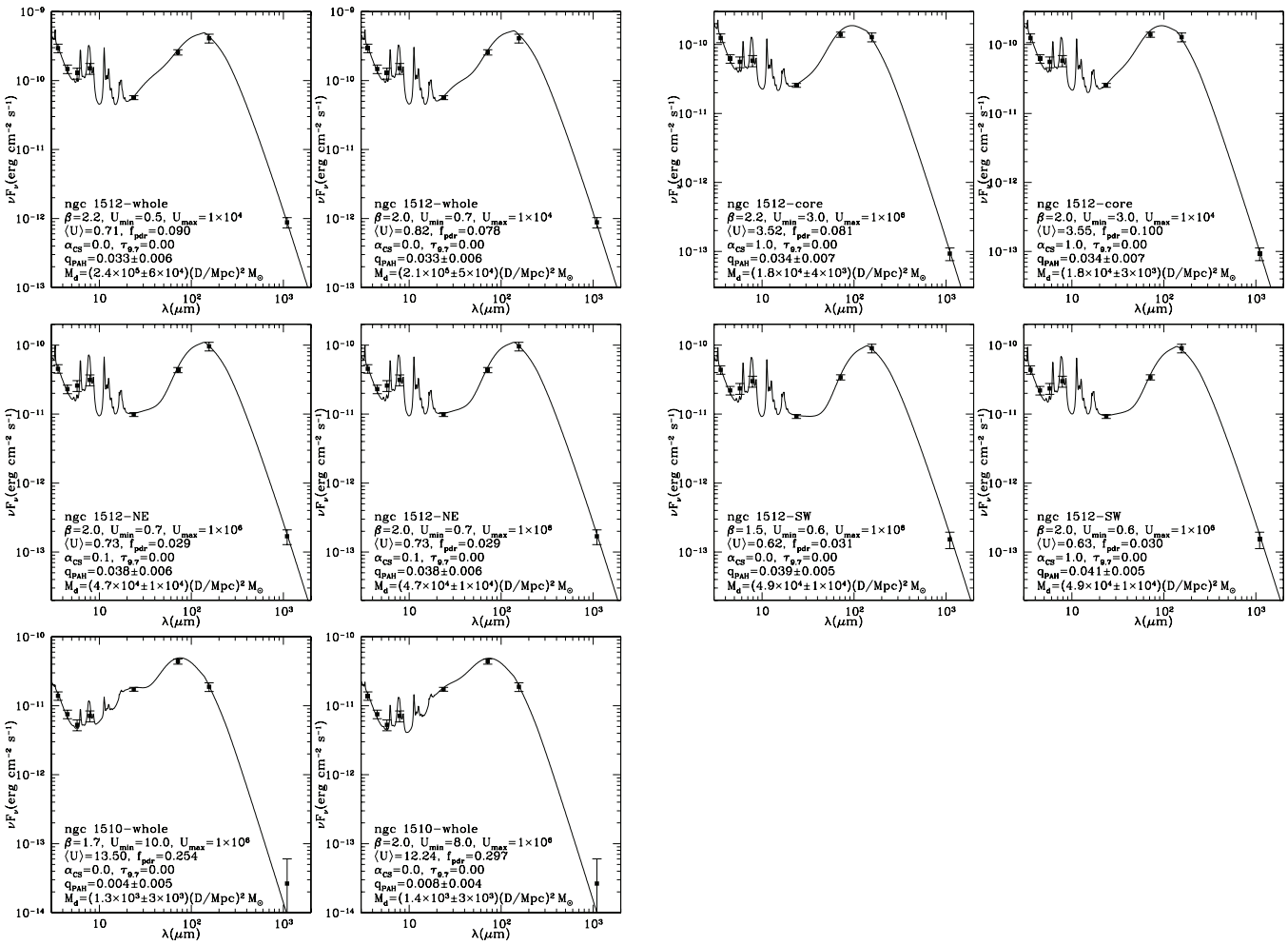

Figure 4. SEDs of NGC 1512, its central region, its northwest and southwest arm regions, and its companion NGC 1510. All the SEDs are fitted by the model described in Draine & Li (2007). The results of two approaches of the fit are shown in a parallel manner: the left panel in each pair allows the parameter β to float between 1.5 and 2.5 freely, but it is fixed for the right. However, the results sometimes coincide with each other.

fit its SED. This is a well-known result: low-mass galaxies tend to have higher effective dust temperatures than large spirals (Hunter et al. 1989; Dale et al. 2005). The total dust masses derived with the two-temperature method are higher than those derived from the more accurate fits using the Draine & Li (2007) models, by a factor 1.6–2.5 in NGC 1512, and by a factor ∼9 in NGC 1510, or 2.8 if the upper bound of its dust mass is applied (Table 4). Assumptions of lower dust emissivity would yield even higher dust masses from the two-temperature method than those derived with the Draine & Li (2007) method (see the Conclusions).

For NGC 1512 as a whole, the warmer dust component includes ∼7% of the total dust mass in the galaxy, and the dominant contributor by mass is the cooler dust component (Table 4). However, in the sub-galactic regions of NGC 1512, the warm dust represents a larger fraction of the total dust mass, between ∼17% and ∼40%. This is consistent with the fact that the sub-galactic regions have been selected to encompass actively star-forming areas in the galaxy, and are likely biased toward higher warm dust contents than the average across NGC 1512. In NGC 1510, the mass-dominant dust component is the cool one, with a mass that is about 36 times larger than that of the warmer component; this is perhaps not surprising as the higher warm dust temperature for this galaxy relative to NGC 1512 naturally leads to a much higher emissivity, corresponding to much smaller warm dust mass. Finally, we remark again that the results for this galaxy are highly uncertain, due to the low significance of the millimeter flux determination.

5. DISCUSSION

The availability of millimeter observations for the nearby, star-forming galaxy pair NGC 1512/1510 indicates that the observed infrared/millimeter SED of both galaxies and of the three sub-galactic regions in NGC 1512 analyzed in this paper are consistent with the presence of a relatively cool dust component ($T_c \sim$ 14–16 K; Figure 3), if a power-law index of the dust emissivity $\epsilon = 2$ is assumed. Presence of a non-negligible cool dust component with temperature below 20 K has already been suggested for nearby elliptical galaxies (Haas et al. 1998; Klaas et al. 1997; Leeuw et al. 2004). In M31, a cold dust component with a temperature of 16 ± 2 K seems to be present as well (Odenwald et al. 1998; Genzel & Cesarsky 2000). Confirming the actual existence of this component in our case is difficult, due to the crudeness of the two-temperature models and to the sparseness of the SED sampling. In general, data between 160 μm and ∼1 mm are not available for galaxies, although a few galaxies (including NGC 1512) have been recently observed at wavelengths between 250 μm and 500 μm with BLAST (Wiebe et al. 2009), and more will

Table 3
Derived Quantities for NGC 1512 and NGC 1510

Parameter	NGC 1512	NGC 1512_{C}[a]	NGC 1512_{NE}[a]	NGC 1512_{SW}[a]	NGC 1510
M_d[b]	$2.4 \pm 0.6 \times 10^7$	$2.1 \pm 0.4 \times 10^6$	$5.5 \pm 1.3 \times 10^6$	$5.7 \pm 1.3 \times 10^6$	$1.7 \pm 3.6 \times 10^5$
$M_{\rm H\,I,VLA}$[c]	4.9×10^8	5.4×10^6	4.6×10^7	6.2×10^7	4.7×10^7
$M_{\rm H\,I,Parkes}$[c]	1.7×10^8	1.2×10^7	1.5×10^7	1.0×10^7	1.4×10^7

Notes.
[a] NGC 1512_{C} represents the central region of NGC 1512, while the northeastern/southwestern arms are denoted by NGC 1512_{NE}/NGC 1512_{SW}.
[b] Derived dust mass, in units of $M_\odot$, from the model fits of Draine et al. (2007).
[c] Extrapolated H I mass, in units of $M_\odot$ (M. D. Thornley 2006, private communication). The total H I mass is the sum of $M_{\rm H\,I,VLA}$ and $M_{\rm H\,I,Parkes}$.

Table 4
Derived Parameters of Two-Blackbody Fit for NGC 1512 and NGC 1510

Parameter	NGC 1512	NGC 1512_{C}[a]	NGC 1512_{NE}[a]	NGC 1512_{SW}[a]	NGC 1510
T_w[b]	24.0	24.8	21.4	20.4	36.1
T_c[b]	13.8	16.2	13.9	13.8	15.4
M_w[c]	4.1×10^6	1.7×10^6	1.8×10^6	2.3×10^6	4.2×10^4
M_c[c]	5.5×10^7	2.5×10^6	8.7×10^6	7.1×10^6	1.5×10^6

Notes.
[a] NGC 1512_{C} represents the central region of NGC 1512, while the northeastern/southwestern arms are denoted by NGC 1512_{NE}/NGC 1512_{SW}.
[b] Best-fit values for the temperatures, T_w and T_c in units of K, from a simple two modified blackbody fit, with fixed power-law index of the dust emissivity $\epsilon = 2$.
[c] Best-fit warm and cool dust masses, in units of $M_\odot$, associated with T_w and T_c, respectively.

become available thanks to the observations with the Herschel Space Telescope. Interestingly, even very actively star-forming galaxies, like LIRGs and ULIRGs, do seem to require some cool dust component, with temperature of order 20 K, about a factor 2–2.5 smaller than the temperature of the warm dust component that dominates the total luminosity (Dunne & Eales 2001).

The observed far-infrared/millimeter SEDs of the two galaxies cannot be easily fit by a single modified blackbody, without requiring that the dust has a power-law index <2: NGC 1512 requires $\epsilon \sim 1.3$ and NGC 1510 $\epsilon \sim 1.1$, the latter value being at the margin of the acceptable range for dust emissivity ($1 \leqslant \epsilon \leqslant 2$; Seki & Yamamoto 1980). Less stringent are the fits of the sub-galactic regions, where the single-temperature assumption requires $\epsilon \sim 1.5$–1.8, marginally consistent with $\epsilon = 2$; indeed, these regions have been selected to be actively star forming, so it is not surprising that their infrared emission is dominated by the warm dust component.

Dust emissivity values $\epsilon < 2$ have been derived for dust emitting regions in the Magellanic Clouds (Aguirre et al. 2003), assuming a single temperature for the modified blackbody; however, two-temperature models with $\epsilon = 2$ appear to produce equally good fits to the data (Aguirre et al. 2003). Furthermore, the multi-wavelength infrared/submillimeter data of ULIRGs and SLUGS galaxies seem to indicate that better fits are obtained when multiple-temperature modified blackbody emission with emissivity having a power-law index $\epsilon = 2$ (Dunne & Eales 2001; Willmer et al. 2009). The presence of multiple-temperature dust components is supported by the recent conclusions of Rieke et al. (2009) and Calzetti et al. (2009), who find evidence for dust self-absorption in the mid-infrared SEDs of LIRGs, which then requires re-emission at longer wavelengths. These results provide ground for an "onion-peel" scenario, where different dust layers are heated at different temperatures.

Single-temperature fits yield values around 20–25 K and ~36 K for the warm dust components of NGC 1512 (and its sub-regions) and NGC 1510, respectively. This is consistent with NGC 1510 being, on average, more actively star-forming than NGC 1512, when considering the star formation rate density (Table 1), and also being less metal-rich, which leads to less ability of self-shielding for the dust (Calzetti et al. 2000). We also notice a higher temperature of the warmer dust in the center of NGC 1512 (25 K) compared to that of the arm regions of the same galaxy (20–21 K), implying a stronger radiation field in the galaxy center where more UV photons are reprocessed by dust grains.

The combination of a long-wavelength baseline for the dust emission (thanks to the millimeter data) and the physically motivated models (Draine & Li 2007) enables us to derive accurate dust masses for NGC 1512 and its sub-regions: typical 1σ uncertainties are in the range 19%–25% (Table 3). Less secure is the dust mass of the fainter NGC 1510, with a factor ~3 uncertainty, due to its faint millimeter emission. We should stress that our quoted accuracy is within the context of the Draine & Li (2007) models. Even with this uncertainty, we are in a position of deriving dust-to-gas ratios for the galaxy pair.

The two interacting galaxies, located in the southern sky, do not have any CO (tracer of molecular gas) observations; therefore we will be limited to the derivation of $M_d/M_{\rm H\,I}$ ratio. Interferometric Very Large Array (VLA) observations exist for the pair (M. D. Thornley 2006, private communication), in addition to single-dish data from the Parkes Telescope (as part of the HIPASS survey; Koribalski et al. 2004). We use the latter data with low angular resolution to recover the diffuse emission in the galaxy pair which is missed by the interferometric data. The Parkes data contain a total emission of 259 ± 17 Jy km s^{-1} at 21 cm, and by comparing this figure with the total flux ($>3\sigma$) contained in the VLA map, we estimate that the interferometric observations miss ~52% of the total H I gas mass. We assume this "diffuse" component to be homogeneously distributed within the area occupied by the two galaxies; this assumption is very simplistic, but we expect that its impact on the individual regions (which are dominated by the clustered H I detected

by the VLA) will not be large, except for the center of NGC 1512 where the H I flux is weak. We then measure the 21 cm emission within each of the five regions defined in Table 2 from the VLA image, include the correction for the "diffuse" gas derived above, and derive H I masses using the conventional formula $M_{\rm H\,I}/M_{\odot} = 2.36\times10^{5} I_{21\,\rm cm} D^{2}_{\rm Mpc}$, where the integrated intensity $I_{21\,\rm cm}$ is in Jy km s^{-1} and the distance in Mpc.

When enclosing the entire H I emission from the NGC 1512/NGC 1510 pair, we obtain $M_d/M_{\rm H\,I} = 0.0034 \pm 0.0008$, consistent with the value 0.0028 found by Draine et al. (2007). If only the H I emission inside our photometry aperture for NGC 1512 itself (see description in the data analysis section) is taken into account, the $M_d/M_{\rm H\,I}$ ratio becomes an order of magnitude higher (0.037). Significantly higher values are obtained for the northern ($M_d/M_{\rm H\,I} = 0.089$) and southern ($M_d/M_{\rm H\,I} = 0.079$) arm regions, and for the core ($M_d/M_{\rm H\,I} = 0.13$). These values should be, however, considered upper limits to the actual dust-to-gas ratios, since we do not have H_2 measurements, and molecular gas is likely to be an important component in these three actively star-forming regions. Based on spatially resolved CO studies of other massive star-forming galaxies (e.g., Kennicutt et al. 2007; Leroy et al. 2008), we estimate the H_2 contribution to the gas content of the sub-galactic regions in NGC 1512 to be at least of the same order as the H I itself. Using the expected proportionality between the dust-to-gas ratio and metallicity in galaxies, $M_d/M_{\rm gas} \approx 0.010({\rm O/H})/({\rm O/H})_{\rm MW}$, from Draine et al. (2007), we can tentatively compare this formula with our derived dust and H I masses. Using the metallicity value in Table 1, we find for NGC 1512, $M_d/M_{\rm gas} = 0.011$, which is lower than the $M_d/M_{\rm H\,I}$ value, we determine the galaxy. We attribute this discrepancy to the absence of molecular gas data. For NGC 1510, we derive $M_d/M_{\rm H\,I} = 0.0027$, and from its metallicity (Table 1) and Draine et al. (2007)'s formula, an expected $M_d/M_{\rm gas} = 0.0042$. Again, although the two numbers differ by about a factor of 2, lack of molecular gas information hampers detailed comparisons.

While $M_d/M_{\rm H\,I}$ ratios for individual regions and/or the whole galaxies appear consistent or larger than what one would expect for $M_d/M_{\rm gas}$ as given by Draine et al. (2007), the dust-to-gas ratio of the galaxy pair is lower, by about a factor of 3, than what expected, based on the same formulae. This "deficiency" would be exacerbated by the presence of significant molecular gas in the system. We speculate this deficiency to be due to the presence of a large fraction of H I not associated with the star-forming disk(s) and/or regions within the two galaxies. A solution to this issue will require both higher sensitivity H I maps and the availability of CO maps to measure the contribution and distribution of the molecular gas.

6. SUMMARY

The combination of *Spitzer* mid/far-infrared images with ground-based ASTE/AzTEC 1.1 mm data for the galaxy pair NGC 1512/1510 has enabled us to derive accurate (∼19%–25% uncertainty) dust masses for the large spiral NGC 1512 and three of its sub-regions (the center and the two spiral arms), and constrain the dust mass of the low-metallicity dwarf galaxy NGC 1510 to within a factor of 3. The total dust mass of NGC 1512 is 2.4×10^{7} $M_{\odot}$ and it is about 150 times smaller in NGC 1510, in agreement with the former being a large spiral galaxy and the latter a small compact dwarf galaxy.

In both galaxies, when the SEDs are fitted with simplistic two-component modified Planck functions, the majority of the dust mass is found to have a relatively cool temperature, ∼14–16 K, similar to what found for the nearby galaxy M31. Conversely, in the central region of NGC 1512 the cool and warm ($T_w \sim 25$ K) dust contribute close to equal mass, reflecting the larger specific star formation rate (SFR) of the starbursting center relative to the galaxy as a whole. The two arm regions display properties that are intermediate between the central region and the whole galaxy in terms of ratio between the warm and cool dust mass, with values in the range 0.2–0.3.

The dust-to-gas ratio in NGC 1512 (estimated using only H I, because of lack of CO emission data for the pair) is about 3 times below the expectation for a galaxy with a metallicity similar to the Milky Way, as already remarked in Draine et al. (2007). The addition of H_2 to the gas census would only make the discrepancy worse. Conversely, the sub-regions (center and arms) in the galaxy show high $M_d/M_{\rm H\,I}$ ratios, ∼0.08–0.09 for the arms and ∼0.13 in the center, thus about 20–30 times larger than the galaxy as a whole, and consistent with the lack of H_2 information. We speculate that much of the H I included in the $M_d/M_{\rm H\,I}$ ratio estimate of the galaxy as a whole is not related to the star-forming disk.

The ASTE project is driven by the Nobeyama Radio Observatory (NRO), a branch of the National Astronomical Observatory of Japan (NAOJ), in collaboration with the University of Chile, and Japanese institutes including the University of Tokyo, Nagoya University, Osaka Prefecture University, Ibaraki University, and Hokkaido University. A part of this study was supported by the MEXT Grant-in-Aid for Specially promoted Research (No. 20001003). K.S. was supported, in part, through the NASA GSFC Cooperative Agreement NNG04G155A.

REFERENCES

Aguirre, J. E., et al. 2003, ApJ, 596, 273
Calzetti, D., Armus, L., Bohlin, R. C., Kinney, A. L., Koornneef, J., & Storchi-Bergmann, T. 2000, ApJ, 533, 682
Calzetti, D., et al. 2005, ApJ, 633, 871
Calzetti, D., et al. 2009, ApJ, submitted
Dale, D. A., et al. 2005, ApJ, 633, 857
Dale, D. A., et al. 2007, ApJ, 655, 863
Dole, H., et al. 2006, A&A, 451, 417
Draine, B. T., & Li, A. 2007, ApJ, 657, 810
Draine, B. T., et al. 2007, ApJ, 633, 866
Dunne, L., & Eales, S. A. 2001, MNRAS, 327, 697
Dunne, L., Eales, S., Edmunds, M., Ivison, R., Alexander, P., & Clements, D. L. 2000, MNRAS, 315, 115
Engelbracht, C. W., et al. 2007, PASP, 119, 994
Ezawa, H., Kawabe, R., Kohno, K., & Yamamoto, S. 2004, Proc. SPIE, 5489, 763
Ezawa, H., et al. 2008, Proc. SPIE, 7012, 701208
Genzel, R., & Cesarsky, C. J. 2000, ARA&A, 38, 761
Gordon, K. D., et al. 2007, PASP, 119, 1019
Haas, M., Lemke, D., Stickel, M., Hippelein, H., Kunkel, M., Herbstmeier, U., & Mattila, K. 1998, A&A, 338, L33
Hunter, D. A., Gallagher, J. S., Rice, W. L., III, & Gillett, F. C. 1989, ApJ, 336, 152
Kamazaki, T., et al. 2005, in ASP Conf. Ser., Vol. 347, The Remote Control System for the ASTE Telescope, ed. P. Shopbell, M. Britton, & R. Ebert (San Francisco, CA: ASP), 533
Kennicutt, R. C., Jr., et al. 2003, PASP, 115, 928
Kennicutt, R. C., et al. 2007, ApJ, 671, 333
Kennicutt, R. C., et al. 2009, ApJ, 703, 1672
Klaas, U., Haas, M., Heinrichsen, I., & Schulz, B. 1997, A&A, 325, L21
Koribalski, B. S., et al. 2004, AJ, 128, 16
Leeuw, L. L., Sansom, A. E., Robson, E. I., Haas, M., & Kuno, N. 2004, ApJ, 612, 837
Leroy, A. K., Walter, F., Brinks, E., Bigiel, F., de Blok, W. J. G., Madore, B., & Thornley, M. D. 2008, AJ, 136, 2782

Moustakas, J., Kennicutt, R. C., Calzetti, D., Dale, D. A., Prescott, M., Smith, J. D. T., & Tremonti, C. A. 2009, ApJ, submitted
Odenwald, S., Newmark, J., & Smoot, G. 1998, AJ, 500, 554
Perera, T. A., et al. 2008, MNRAS, 391, 1227
Rieke, G. H., Alonso-Herrero, A., Weiner, B. J., Perez-Gonzalez, P. G., Blaylock, M., Donley, J. L., & Marcillac, D. 2009, ApJ, 692, 556
Scott, K. S., et al. 2008, MNRAS, 385, 2225
Seaquist, E., Yao, L., Dunne, L., & Cameron, H. 2004, MNRAS, 349, 1428
Seki, J., & Yamamoto, T. 1980, Ap&SS, 72, 79
Stansberry, J. A., et al. 2007, PASP, 119, 1038
Storchi-Bergmann, T., Calzetti, D., & Kinney, A. 1994, ApJ, 429, 572
Vlahakis, C., Dunne, L., & Eales, S. 2005, MNRAS, 364, 1253
Weingartner, J. C., & Draine, B. T. 2001, ApJ, 548, 296
Wiebe, D. V., et al. 2009, ApJ, 707, 1809
Willmer, C. N. A., Rieke, G. H., Le Floc'h, E., Hinz, J. L., Engelbracht, C. W., Marcillac, D., & Gordon, K. D. 2009, AJ, 138, 146
Wilson, G. W., et al. 2008a, MNRAS, 386, 807
Wilson, G. W., et al. 2008b, MNRAS, 390, 1061